

Cyanolysis and Azidolysis of Epoxides by Haloalcohol Dehalogenase: Theoretical Study of the Reaction Mechanism and Origins of Regioselectivity[†]

Kathrin H. Hopmann and Fahmi Himo*

Department of Theoretical Chemistry, School of Biotechnology, Royal Institute of Technology, AlbaNova University Center, SE-106 91 Stockholm, Sweden

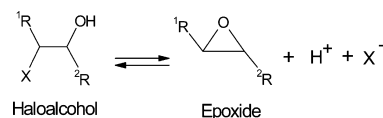
Received January 1, 2008; Revised Manuscript Received February 12, 2008

ABSTRACT: Haloalcohol dehalogenase HheC catalyzes the reversible dehalogenation of vicinal haloalcohols to form epoxides and free halides. In addition, HheC is able to catalyze the irreversible and highly regioselective ring-opening of epoxides with nonhalide nucleophiles, such as CN^- and N_3^- . For azidolysis of aromatic epoxides, the regioselectivity observed with HheC is opposite to the regioselectivity of the nonenzymatic epoxide-opening. This, together with a relatively broad substrate specificity, makes HheC a promising tool for biocatalytic applications. We have designed large quantum chemical models of the HheC active site and used density functional theory to study the reaction mechanism of the HheC-catalyzed ring-opening of (*R*)-styrene oxide with the nucleophiles CN^- and N_3^- . Both the cyanolysis and the azidolysis reactions are shown to take place in a single concerted step. The results support the suggested role of the putative Ser132-Tyr145-Arg149 catalytic triad, where Tyr145 acts as a general acid, donating a proton to the substrate, and Arg149 interacts with Tyr145 and facilitates proton abstraction, while Ser132 positions the substrate and reduces the barrier for epoxide opening through interaction with the emerging oxyanion of the substrate. We have also studied the regioselectivity of (*R*)-styrene oxide opening for both the cyanolysis and the azidolysis reactions. The employed active site model was shown to be able to reproduce the experimentally observed β -regioselectivity of HheC. *In silico* mutations of various groups in the HheC active site model were performed to elucidate the important factors governing the regioselectivity.

Haloalcohol dehalogenases (also referred to as halohydrin dehalogenases) catalyze the reversible dehalogenation of vicinal haloalcohols, thereby forming the corresponding epoxides and free halides (Scheme 1). They have been identified in different microbes, including *Corynebacterium* sp. (1), *Arthrobacter* sp. (2, 3), *Agrobacterium radiobacter* (3), and *Mycobacterium* sp. (3). Structural studies have shown that haloalcohol dehalogenases are closely related to the superfamily of NAD(P)H-dependent short-chain dehydrogenase/reductases (SDRs¹) (3, 4). However, the haloalcohol dehalogenase reaction is cofactor-independent, and instead of the nicotinamide binding site found in the SDRs, the haloalcohol dehalogenases exhibit a distinct halide-binding site (4).

The reaction mechanism of haloalcohol dehalogenases is proposed to be mediated by a catalytic Ser-Tyr-Arg triad, which is similar to the Ser-Tyr-Lys triad found in the SDRs (3, 4). Mutational studies of haloalcohol dehalogenase HheC from *Agrobacterium radiobacter* AD1 have confirmed the importance of the catalytic triad for activity (3). In the

Scheme 1: Haloalcohol Dehalogenase Reaction



dehalogenation mechanism, it is suggested that Arg149 abstracts a proton from Tyr145, which in turn abstracts a proton from the haloalcohol substrate (Scheme 2, numbering as in HheC). An intramolecular displacement reaction then results in the formation of an epoxide. The liberated halide is stabilized by various interactions in the halide binding site, for example, with the backbone amide of Leu178 and a water molecule (4). The dehalogenation reaction is reversible, with the reverse step leading to epoxide-opening (5). Interestingly, in the epoxide-opening reaction, nucleophiles other than halides, such as NO_2^- , CN^- , and N_3^- , are accepted by HheC (6–11). With azide and cyanide, HheC-mediated transformation of epoxides results in the irreversible formation of β -azidoalcohols and β -hydroxynitriles, respectively (11, 10). With nitrite as nucleophile, unstable hydroxynitrite esters are formed, which are readily hydrolyzed to the corresponding diols (9).

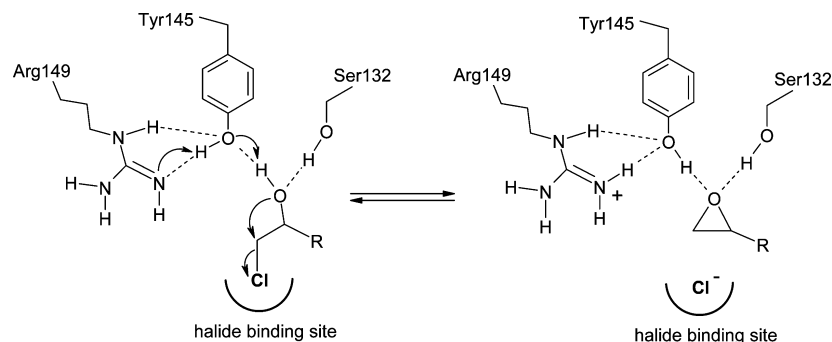
The high regio- and stereoselectivity of HheC, combined with its relatively broad substrate specificity make it promising as a versatile and selective biocatalyst (10–13). HheC preferably reacts with the (*R*)-enantiomer of various substituted styrene oxides and haloalcohols (5, 9, 13). Kinetic resolution of *p*-nitro-styrene oxide using HheC and nitrite

[†] We gratefully acknowledge financial help from The Swedish Research Council, The Wenner-Gren Foundations, The Carl Trygger Foundation, and The Magn Bergvall Foundation.

* Corresponding author. Tel: +46 8-55378415. Fax: +46 8-55378590. E-mail: himo@theochem.kth.se.

¹ Abbreviations: CPCM, conductor-like polarizable continuum model; DFT, density functional theory; RPAE, (*R*)-1-phenyl-2-azido-ethanol; RpNPAE, (*R*)-1-*para*-nitro-phenyl-2-azido-ethanol; RSO, (*R*)-styrene oxide; SDR, short-chain dehydrogenase/reductase; ZPV, zero-point vibrational; TS, transition state.

Scheme 2: Proposed Dehalogenation Reaction Mechanism for HheC (3)



exhibited an E-value of 200. The remaining (*S*)-epoxide was obtained with an enantiomeric excess (ee) of >99% (9). HheC has also been used on the preparative scale for kinetic resolution of 3-alkenyl and heteroaryl chloroalcohols, with resulting ee values of >99% (13).

In the epoxide opening reaction with the nonhalide nucleophiles, NO_2^- , CN^- , and N_3^- , HheC exhibits high β -regioselectivity (9–11). For the azidolysis of aromatic epoxides, this β -regioselectivity of HheC differs from the α -regioselectivity observed for the nonenzymatic epoxide opening in water (10). This makes HheC very useful for the formation of β -azidoalcohols (10).

Detailed understanding of the reaction mechanism and the origins for the displayed regioselectivity of HheC could be of great aid in designing new epoxide-transforming reactions with this enzyme.

In the present article, we use density functional theory (DFT) to investigate the epoxide-opening reaction of HheC. Large quantum chemical models based on the X-ray crystal structure of HheC (4) are employed to study the reaction of (*R*)-styrene oxide (RSO) with the nucleophiles CN^- and N_3^- . The role of the proposed catalytic triad Ser132-Tyr145-Arg149 in the epoxide-opening reaction is analyzed. Also the regioselectivity of the cyanolysis and azidolysis of RSO is investigated. The large size of the active site model allowed us to make several *in silico* mutations to explore the roles of the various active site residues in controlling the regioselectivity. A similar modeling approach has been used previously to investigate a number of other enzyme reaction mechanisms (14).

COMPUTATIONAL DETAILS

All calculations were performed using the hybrid density functional theory method B3LYP (15), as implemented in Gaussian03 (16). Geometries were optimized using the 6-31G(d,p) basis set. Energies were calculated by performing single point calculations on the optimized geometries using the 6-311+G(2d,2p) basis set. These large basis set energies were corrected for solvation effects due to the surrounding environment. The solvation corrections were calculated at the same level of theory as optimizations by performing single point calculations using the conductor-like polarizable continuum model (CPCM) (17). For the HheC active site models, a dielectric constant of $\epsilon = 4$ was used, which is the standard value used in protein modeling. The effect of using other dielectric constants was investigated for one of the reactions, and the results were shown to be quite insensitive to the choice of ϵ . These results are given in the

Supporting Information. For the nonenzymatic phenol-catalyzed models, a dielectric constant of $\epsilon = 80$ was employed. Frequency calculations were performed on the optimized structures of the phenol-catalyzed model at the same level of theory to determine zero-point vibrational (ZPV) effects. For the HheC active site models, the ZPV effects were not calculated explicitly, but were transferred from the phenol-catalyzed model. The final energies presented here are the large basis set energies corrected for solvation and ZPV effects.

ACTIVE SITE MODEL

The quantum chemical model employed in this study is based on the X-ray crystal structure of wild-type HheC in complex with the product (*R*)-1-*para*-nitro-phenyl-2-azidoethanol (*R*pNPAE), PDB code 1PXO (4). Important active site residues were extracted from the PDB file and truncated (Figure 1 and Table 1). Hydrogen atoms were added manually. In the geometry optimizations, truncation atoms were fixed to their crystallographically observed positions. The residues included in the model are the putative catalytic triad Ser132-Tyr145-Arg149 and parts of the residues that constitute the halide binding site in HheC (see Figure 1 and Table 1). In this study, we assume that the epoxide opening corresponds to the reverse of the dehalogenation reaction (Scheme 2), i.e., with Tyr145 acting as the catalytic acid and with Arg149 as the proton donor to Tyr145. Both Arg149 and Tyr145 were thus modeled in their protonated forms. This is a reasonable assumption, considering that the pH optimum for the epoxide opening reaction of HheC is about 4–5 (4).

The halide binding site in HheC is mainly formed by the residues Pro175, Asn176, Tyr177, Leu178, Phe12, Tyr185, Phe186, and Tyr187 (4). From the X-ray crystal structure, it is suggested that the halide ion forms hydrogen bonds with the backbone amides of Leu178 and Tyr177 and with a water molecule located in the active site (4). The water molecule also interacts with the backbone carbonyl of Leu178 (4). The water molecule and the backbone parts of Pro175, Asn176, Tyr177, and Leu178 were included in the active site model (Figure 1 and Table 1). For Asn176, the entire side-chain was kept in the model, as this is involved in interactions with the phenol moiety of Tyr187, which was also included in the model. The interaction between Asn176 and Tyr187 is suggested to play a role in stabilizing the conformation of the halide binding site (4, 26). Additionally, parts of the side chains of Phe12 and Phe187 were included in the model.

HheC has broad substrate specificity and accepts various aliphatic and aromatic epoxides as substrates, including

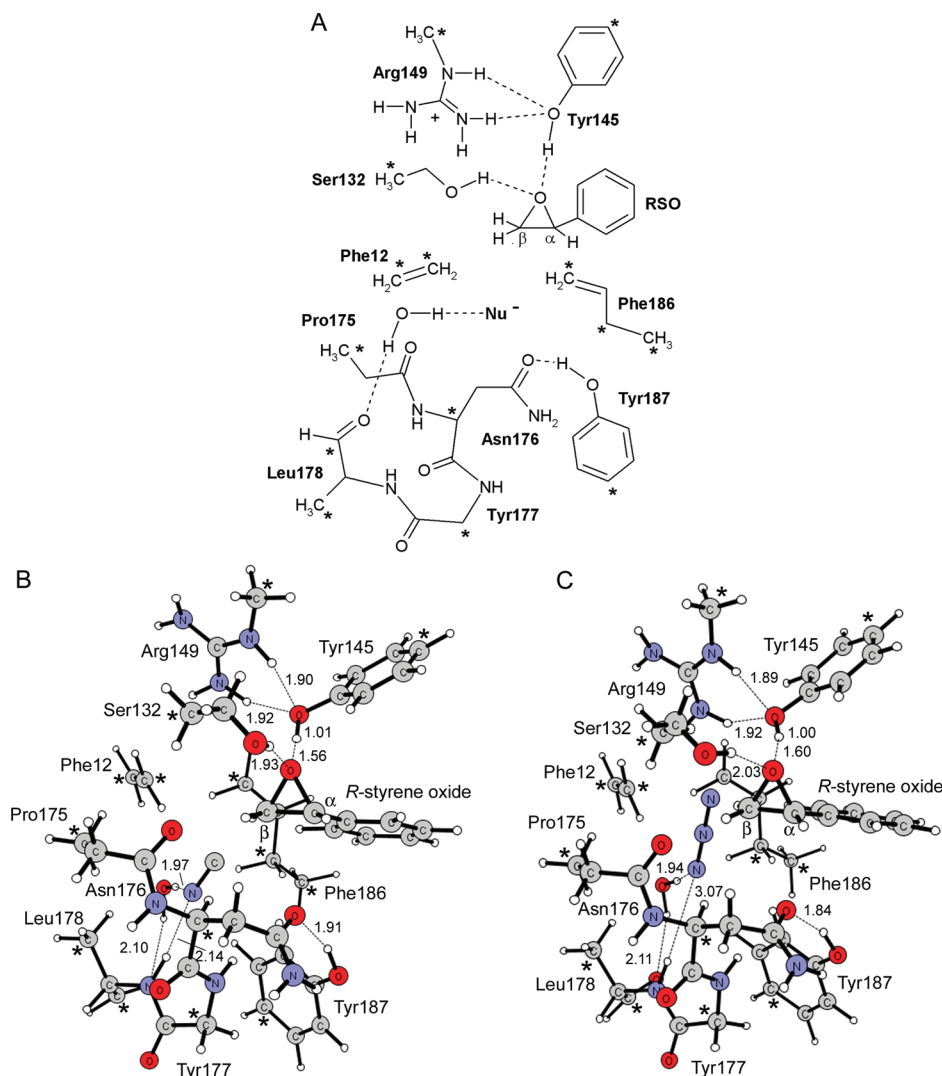


FIGURE 1: HheC active site model used in the present study. (A) Schematic drawing showing the details of the chemical composition. (B) Optimized reactant structure with cyanide and RSO. (C) Optimized reactant geometry with azide and RSO. Asterisks mark atoms kept fixed to their crystallographic position in optimizations. Distances are in Ångströms.

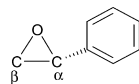
Table 1: Description of the Wild-Type HheC Active Site Model Used in the Present Study

	part included from X-ray crystal structure (1PXO)	proposed function/role in the model	fixed at position ^a
Ser132	C α + side chain	positions the substrate	C α
Tyr145	phenol	general acid	C γ
Arg149	<i>N</i> -methyl-guanidine	activates Tyr145	C δ
Pro175	C=O, C α , C β	part of halide binding site	C β
Asn176	entire backbone + side chain	part of halide binding site	C α
Tyr177	backbone (N, C α , C=O)	part of halide binding site	C α
Leu178	backbone (N, C α , C=O) + C β	part of halide binding site	C β
Phe186	C α , C β , C γ , C δ	part of halide binding site	C α , C β , C δ
Tyr187	phenol	part of halide binding site	C γ
Phe12	C γ , C δ	part of halide binding site	C γ , C δ
H ₂ O	water	part of halide binding site	
RSO ^b	parts of R _p NPAE ^c	substrate	
CN ⁻ or N ₃ ⁻		nucleophile	

^a These atoms were kept fixed to their crystallographically observed positions during geometry optimizations. ^b (*R*)-styrene oxide. ^c (*R*)-1-*para*-nitro-phenyl-2-azido-ethanol.

styrene oxide (10). The (*R*)-enantiomer of styrene oxide (RSO) is the preferred substrate, while the (*S*)-enantiomer shows basically no activity (10). We used RSO as substrate in our studies of HheC (Scheme 3). In the HheC-mediated azidolysis of RSO, the main product is (*R*)-1-phenyl-2-azido-ethanol (RPAE), while (*R*)-1-phenyl-1-azido-ethanol is a minor product (10). To model the azidolysis reaction of HheC

with RSO, we modified the crystallographically observed (*R*)-1-*para*-nitro-phenyl-2-azido-ethanol (R_pNPAE) into RPAE by removing the nitro group of R_pNPAE. The resulting model of the wild-type HheC active site with the product RPAE has a size of 130 atoms. From this model, the reactant structure containing RSO and the free azide nucleophile was modeled. For the cyanolysis reaction, azide was replaced with

Scheme 3: (*R*)-Styrene Oxide (RSO) Substrate Used in the Current Study

cyanide in the model. Including the charge of the nucleophile, the active site models described in the text have a total charge of 0.

The nonenzymatic acid-catalyzed cyanolysis and azidolysis reactions of RSO were also studied with a small model consisting of the substrate, the nucleophile and a phenol molecule as acid (see below). The phenol-catalyzed model has an overall charge of -1 and a size of 32–33 atoms, depending on the nucleophile.

RESULTS AND DISCUSSION

Reaction Mechanism. The epoxide-opening mechanism of HheC was studied using the active site model described

above (also see Figure 1A). First, we modeled the cyanolysis and azidolysis of (*R*)-styrene oxide (RSO) involving attack at the terminal carbon ($C\beta$) of the substrate. In the optimized reactant structure for the cyanolysis reaction (Figure 1B), the cyanide is bound in the halide binding site, where it forms two hydrogen bonds, one to the Leu178 backbone amide with a length of 3.15 Å and one to the water molecule with a length of 2.94 Å (hydrogen bond length here refers to the distance between donor and acceptor atoms). The epoxide substrate is positioned above the halide binding site, where it is hydrogen-bonded to Tyr145 and Ser132 with bond lengths of 2.57 Å and 2.88 Å, respectively. The third residue of the putative catalytic triad, Arg149, forms two hydrogen bonds to Tyr145, one from the $N\epsilon$ and one from the $N\eta$.

The transition state (TS) for nucleophilic attack of cyanide at the terminal carbon ($C\beta$) of RSO was optimized, and the structure is shown in Figure 2A. The calculated barrier for this step is 7.0 kcal/mol. At the TS, the distance between the cyanide and the β -carbon is 2.32 Å. The epoxide is

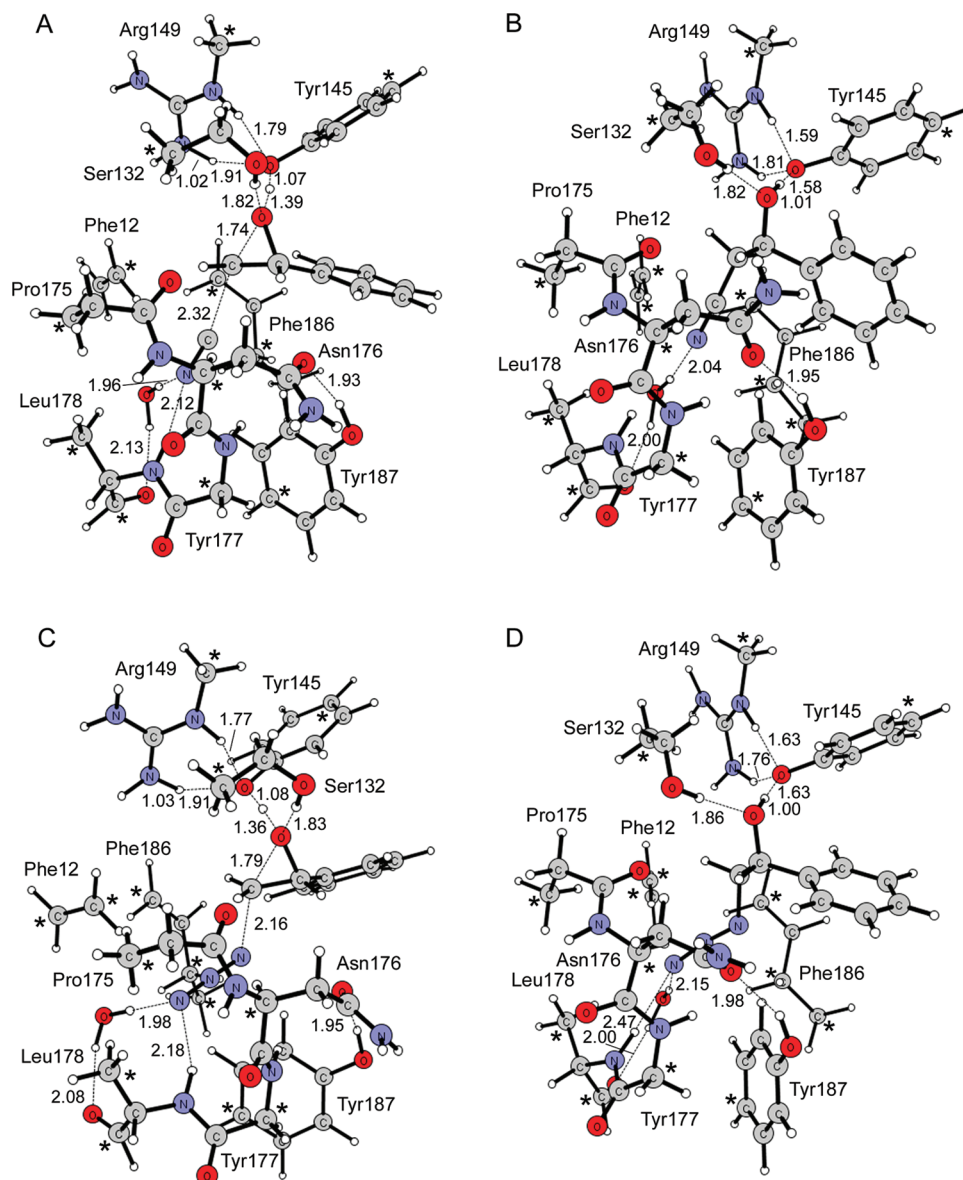


FIGURE 2: Optimized geometries for cyanolysis or azidolysis of RSO in the HheC active site model, attack at $C\beta$. (A) Transition state for cyanolysis. (B) Product structure with the formed cyanoalcohol. (C) Transition state for azidolysis. (D) Product structure with the formed azidoalcohol.

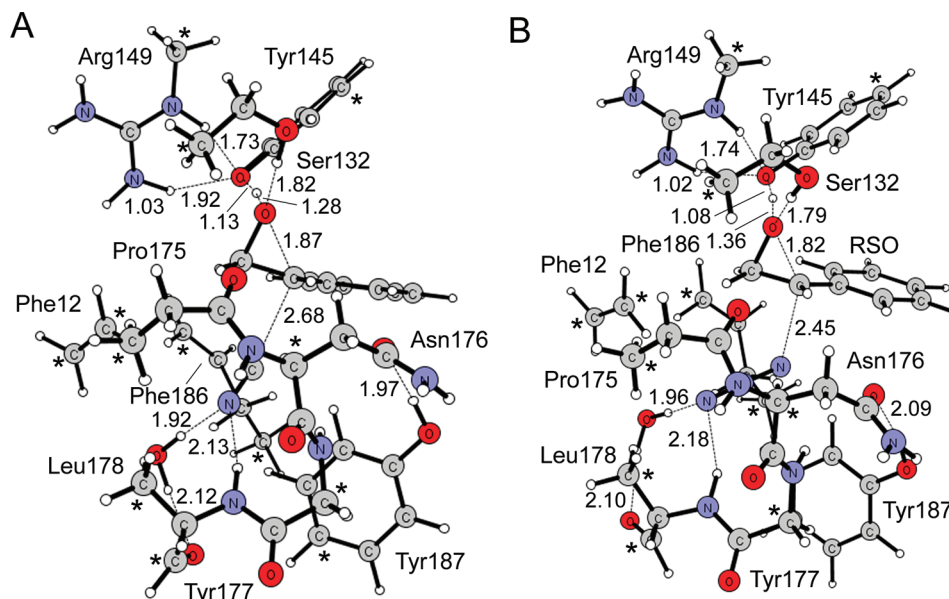


FIGURE 3: Optimized transition states for epoxide opening at C α of RSO in the wild-type HheC active site model. (A) Cyanolysis. (B) Azidolysis.

partially opened with an O–C β distance of 1.74 Å. The optimized structure reveals that proton transfer from Tyr145 occurs in concert with epoxide opening, as suggested in Scheme 2. The Tyr145 O–H bond is elongated to 1.07 Å, and the proton is located only 1.39 Å from the epoxide oxygen. A proton transfer from Arg149 to Tyr145 is not evident from the optimized TS. However, the interaction with Arg149 promotes the formation of a tyrosinate. Ser132 seems to aid in the stabilization of the transient epoxide oxyanion. The hydrogen bond between Ser132 and the epoxide oxygen has changed from 2.88 Å in the reactant to 2.79 Å in the transition state. In the product geometry with the cyanoalcohol (Figure 2B), the proton from Tyr145 has been transferred fully to the alcohol, and the formed tyrosinate interacts with Arg149 through two hydrogen bonds. The cyanide moiety of the product is bound in the halide binding site, where it forms a hydrogen bond with the water molecule, but has lost its former hydrogen bond to the backbone of Leu178. The reaction is calculated to be exothermic by as much as 46.0 kcal/mol, in line with the observed irreversibility of HheC-mediated cyanolysis of epoxides (7).

Analogously, we studied the azidolysis of RSO with the same HheC active site model by exchanging the cyanide molecule with azide. Azide is a slightly larger nucleophile than cyanide, and consequently, its interactions in the active site are slightly different (Figure 1C). As with cyanide, the azide forms a hydrogen bond to the water molecule. However, the interaction with the Leu178 backbone amide is now considerably weaker, with a donor–acceptor distance of 4.06 Å. Another important difference is that the azide has positioned itself closer to the positively charged Arg149 (see Figure 1C).

The azidolysis reaction proceeds in a similar fashion as described above for cyanide as nucleophile. At the transition state (Figure 2C), the distance between the azide and the β -carbon is 2.16 Å and the O–C β distance is 1.79 Å. The Tyr145 oxygen–hydrogen bond has an elongated length of 1.08 Å and the proton is 1.36 Å from the epoxide oxygen. Proton transfer from Tyr149 does thus occur in concert with

nucleophilic attack, as for the cyanolysis reaction. The calculated barrier is 8.1 kcal/mol and the reaction energy is –25.2 kcal/mol, which also here is in line with the observed irreversibility of HheC-mediated azidolysis (10).

To summarize this section, the barriers and reaction energies calculated for both the cyanolysis and azidolysis reactions of RSO in the HheC active site model establish the feasibility of the assumed reaction mechanism, with Tyr145 acting as general acid and Arg149 and Ser132 assisting in the proton transfer and substrate stabilization.

Epoxide Opening at the Benzylic Carbon. As mentioned above, HheC-catalyzed epoxide opening with cyanide and azide occurs preferably at the terminal carbon (C β) of 1,2-epoxides (10, 11). However, the regioselectivity of attack is not absolute. It is thus also of interest to study the nucleophilic attack at C α of RSO.

We used the same active site model to study the nucleophilic attack of both cyanide and azide at the C α carbon of RSO. The optimized transition states are displayed in Figure 3. The mechanism for opening at the benzylic carbon is the same as for opening at the terminal carbon. That is, nucleophilic attack occurs concertedly with proton transfer from Tyr145. The transition state structures are in general quite similar to the β -attack. One significant difference, however, is that for both cyanolysis and azidolysis: the nucleophile–C α distance is about 0.3 Å longer than the corresponding nucleophile–C β distance. This is, in part, a result of the phenyl substituent at the C α position, which stabilizes the emerging carbocation at that center, making the transition state earlier.

The calculated barrier for azide attack at C α of RSO is 8.6 kcal/mol, which is only 0.5 kcal/mol higher than that for the C β attack. This is in excellent agreement with the experimentally determined regioselectivity for HheC-catalyzed azidolysis of RSO, which shows 79% attack at C β and 21% attack at C α (10). The computed reaction energy is –21.4 kcal/mol, which is 3.8 kcal/mol above the reaction energy for attack at C β .

Cyanide attack at C α of RSO has a calculated barrier of 10.6 kcal/mol, which is 3.6 kcal/mol higher than that for C β attack. This indicates that HheC-mediated cyanolysis of RSO exhibits higher selectivity for the β -carbon than does the azidolysis reaction. Indeed, this is in line with experimental results, which show high β -regioselectivity for HheC-catalyzed cyanolysis of various 1,2-epoxides (11). The computed reaction energy is -40.5 kcal/mol, which is 5.5 kcal/mol higher than the reaction energy for attack at C β .

These results show that the active site model used in the present study is able to reproduce the experimentally determined regioselectivity very accurately. An important reason for this is that when comparing two very similar reactions (like attacks on C α and C β), many systematic errors cancel, and much higher accuracy can thus be obtained.

As discussed above, the regioselectivity of HheC-mediated azidolysis of RSO is opposite of the regioselectivity found for RSO azidolysis in water. Under the same conditions as the enzymatic azidolysis, but in the absence of enzyme, azide attack occurs only to 2% at C β of styrene oxide, while in the enzymatic reaction, attack occurs to 79% at C β (10). The molecular basis for the change of regioselectivity has not been identified.

The fact that our active site model reproduces the experimental results for HheC indicates that the factors governing the regioselectivity are captured within the model. Below, we will identify these factors by making a number of modifications, *in silico* mutations, to the model. However, for better understanding, and as a reference, we will first discuss the regioselectivity of the nonenzymatic azidolysis and cyanolysis of RSO.

Regioselectivity of Nonenzymatic RSO Conversion. The regioselectivity of epoxide opening is normally dependent on multiple factors, including the substitution pattern of the epoxide, the type of nucleophile utilized, and the reaction conditions (18). To understand the intrinsic regioselectivity of cyanolysis and azidolysis of RSO under acidic conditions, we modeled the epoxide opening of RSO using a small model, consisting of the nucleophile, the RSO substrate, and a phenol moiety as an acid. The optimized transition state structures for attacks on C α and C β are presented in Figure 4.

At the transition state for phenol-catalyzed cyanolysis of RSO at the β -carbon, the cyanide carbon is found at a distance of 2.40 Å from C β (Figure 4A). The epoxide is partially opened and exhibits an O–C β distance of 1.70 Å. The transition state for C α attack shows similar distances, with an O–C α bond length of 1.73 Å and a distance to the cyanide carbon of 2.49 Å (Figure 4B). At both transition states, proton transfer occurs concertedly with epoxide opening. The calculated barriers are 11.0 and 10.5 kcal/mol for cyanide attack at C β and C α , respectively, and the reaction energies are -35.7 and -31.1 kcal/mol, respectively. The small difference in barriers suggests that acid-catalyzed cyanolysis of RSO results in a mixture of products, with a slight preference for attack at C α . For cyanolysis of styrene oxide in solution, different regioselectivities have been reported, in most cases leading to a mixture of products (19–24). It is interesting to note that the regioselectivity of RSO cyanolysis computed with the phenol-catalyzed model is significantly different from the regioselectivity calculated for

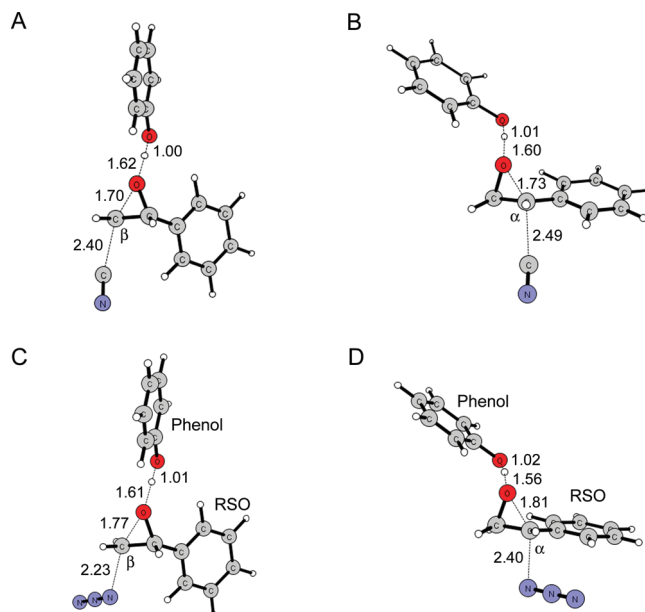


FIGURE 4: Transition states for the attack of cyanide or azide on (*R*)-styrene oxide in the presence of phenol as acid. (A) CN $^-$ attack at C β . (B) CN $^-$ attack at C α . (C) N $_3^-$ attack at C β . (D) N $_3^-$ attack at C α .

Table 2: Calculated Barriers (kcal/mol)^a for the Azidolysis and Cyanolysis of RSO

model (# atoms)	nucleophile	barrier		
		C α	C β	regioselectivity
phenol-catalyzed (32)	CN $^-$	10.5	11.0	+0.5
HheC wild-type (129)	CN $^-$	10.6	7.0	-3.6
HheC Ser132 \rightarrow Ala (128)	CN $^-$	12.1	9.2	-2.9
HheC Leu178NH \rightarrow O (128)	CN $^-$	9.1	6.5	-2.6
HheC Pro175CO \rightarrow CH $_2$ (130)	CN $^-$	10.8	8.5	-2.3
HheC RmTyr187 (116)	CN $^-$	7.9	7.8	-0.1
phenol-catalyzed (33)	N $_3^-$	10.7	13.5	+2.8
HheC wild-type (130)	N $_3^-$	8.6	8.1	-0.5
HheC Ser132 \rightarrow Ala (129)	N $_3^-$	13.1	13.8	+0.7
HheC Leu178NH \rightarrow O (129)	N $_3^-$	10.4	10.5	+0.1
HheC Pro175CO \rightarrow CH $_2$ (131)	N $_3^-$	11.2	11.5	+0.3
HheC RmTyr187 (117)	N $_3^-$	9.2	11.6	+2.4

^a Solvation corrections were calculated with $\epsilon = 80$ for phenol-catalyzed models and $\epsilon = 4$ for HheC active site models.

the HheC-active site model, where a pronounced preference for attack at C β of RSO was found (Table 2).

The optimized transition states for phenol-catalyzed azidolysis of RSO are also shown in Figure 4. At the transition state for C β attack, the epoxide ring is partially opened with a distance of 1.77 Å (Figure 4C). The terminal azide nitrogen attacks the RSO C β at a distance of 2.23 Å. For C α attack, these distances are 1.81 and 2.40 Å, respectively (Figure 4D). At both transition states, the proton from the phenol moiety is transferred concertedly with nucleophilic attack. The barrier for attack of azide at C β is 13.5 kcal/mol, while it is significantly lower for attack at C α with a barrier of 10.7 kcal/mol (Table 2). The reaction energies are -13.2 and -10.8 kcal/mol for attack at C β and C α , respectively. The calculated barriers are in very good agreement with the experimentally determined regioselectivity for the acid-catalyzed azidolysis of RSO in water, which yields 3% attack at C β and 97% attack at C α (25).

The above results show that for both the azidolysis and cyanolysis of RSO, the regioselectivity is changed significantly in going from the phenol-catalyzed to the HheC active

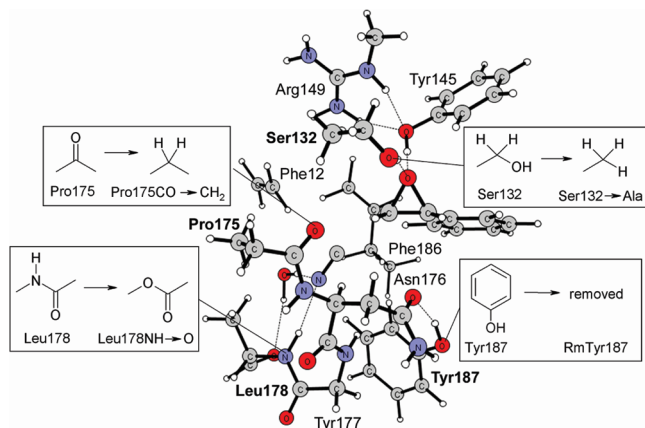


FIGURE 5: Overview of individual *in silico* mutations studied in the HheC active site model.

site model (Table 2). In each case, the HheC-mediated conversion of RSO promotes attack at $C\beta$ with several kcal/mol compared to that for the phenol-catalyzed conversion.

REGIOSELECTIVITY OF HheC

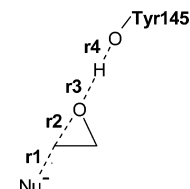
Inspection of the optimized structures for the cyanolysis and azidolysis of RSO in the HheC active site model (Figures 1, 2, and 3) indicates that several groups in the active site might influence the regioselectivity of epoxide opening. In order to understand the individual effect of each group, we changed each one, one at a time, and recalculated the barriers for attack at $C\alpha$ and $C\beta$ of RSO. An overview of the performed *in silico* mutations is given in Figure 5.

It is first interesting to note that in the optimized reactant structures of the native HheC active site with azide or cyanide (Figure 1), the distance from the attacking atom of the nucleophile is considerably shorter to $C\beta$ than to $C\alpha$ of RSO. For cyanide, these distances are 3.47 Å and 4.44 Å, respectively, while for azide, they are 3.49 Å and 4.45 Å, respectively. For a reaction in solution, where the nucleophile and the substrate are not restricted in their movements, a distance difference of this magnitude might be less critical. However, in the HheC active site, large movements of the substrate or the nucleophile might be energetically costly. As discussed above, the substrate and nucleophile are bound to their positions in the active site by a number of hydrogen bonds. We first tested the influence of two of these hydrogen bonds, from Ser132 to the substrate and from Leu178 to the nucleophile, on the barriers and regioselectivity of epoxide opening.

The Ser132 OH group was replaced by a hydrogen atom (equivalent to a Ser132 → Ala mutation) and the geometries and energies were recalculated. The optimized transition states for attack of cyanide or azide at $C\beta$ and $C\alpha$ of RSO in the Ser132 → Ala model are shown in Supporting Information. The computed barriers are compared in Table 2, and critical distances are listed in Table 3.

For the cyanolysis of RSO at the $C\beta$, the critical cyanide- $C\beta$ and $C\beta$ -O distances are very similar to the wild-type model. However, the interaction of the epoxide oxygen with the Tyr145 proton is stronger because the stabilizing effect of Ser132 is now lacking. The same is observed at the α -transition state. The removal of stabilization caused by Ser132 on the emerging epoxide oxyanion is reflected in the barriers, which are calculated to 9.2 and 12.1

Table 3: Critical Transition State Distances (Å) Optimized for Cyanolysis and Azidolysis of (*R*)-Styrene Oxide in the Wild-Type and Mutant Models of HheC



HheC model	attack	nucleophile	r1	r2	r3	r4
wild-type	$C\alpha$	CN^-	2.68	1.87	1.28	1.13
	$C\beta$	CN^-	2.32	1.74	1.39	1.07
Ser132 → Ala	$C\alpha$	CN^-	2.86	1.85	1.08	1.37
	$C\beta$	CN^-	2.32	1.76	1.26	1.15
Leu178NH → O	$C\alpha$	CN^-	2.59	1.83	1.34	1.09
	$C\beta$	CN^-	2.35	1.71	1.40	1.06
Pro175CO → CH_2	$C\alpha$	CN^-	2.72	1.85	1.38	1.07
	$C\beta$	CN^-	2.35	1.72	1.43	1.05
RmTyr187	$C\alpha$	CN^-	2.65	1.86	1.30	1.12
	$C\beta$	CN^-	2.31	1.77	1.42	1.06
wild-type	$C\alpha$	N_3^-	2.45	1.82	1.36	1.08
	$C\beta$	N_3^-	2.16	1.79	1.36	1.08
Ser132 → Ala	$C\alpha$	N_3^-	2.73	1.97	1.05	1.44
	$C\beta$	N_3^-	2.22	1.76	1.13	1.29
Leu178NH → O	$C\alpha$	N_3^-	2.47	1.83	1.35	1.09
	$C\beta$	N_3^-	2.21	1.77	1.37	1.08
Pro175CO → CH_2	$C\alpha$	N_3^-	2.42	1.85	1.38	1.07
	$C\beta$	N_3^-	2.15	1.77	1.41	1.06
RmTyr187	$C\alpha$	N_3^-	2.64	1.88	1.20	1.20
	$C\beta$	N_3^-	2.23	1.78	1.39	1.07

kcal/mol for attack at $C\beta$ and $C\alpha$, respectively. In both cases, the barrier is somewhat raised compared to the wild-type model. The smaller increase for the α -transition state reduces the regioselectivity with 0.7 kcal/mol compared to that of the wild-type (−2.9 vs −3.6 kcal/mol).

Similarly, the effect of the Ser132 → Ala mutation on the azidolysis reaction was also tested in the active site model. The barriers for attacks at $C\alpha$ and $C\beta$ are raised by 4.5 and 5.7 kcal/mol, respectively, compared to those for the wild-type model. This is a somewhat larger increase compared to that in the cyanolysis reaction. The regioselectivity is changed by 1.2 kcal/mol compared to that in the wild-type model (0.5 kcal/mol in favor of β -attack in the wild-type, compared to 0.7 kcal/mol in favor of α -attack in the Ser132 → Ala model).

These results show that the hydrogen-bonding interaction of the Ser132 to the epoxide contributes to the regioselectivity by lowering the barrier for the β -attack compared to that for the α -attack.

It should be noted here that an experimentally prepared Ser132Ala mutant of HheC seems to be completely inactive since no activity could be measured for the dehalogenation of *p*-nitro-2-bromo-1-phenylethanol (3). It can be assumed that the HheC-mediated dehalogenation reaction proceeds through a transition state similar to the epoxide-opening reaction investigated here. Our calculations indicate that this mutation increases the barrier but not to the extent that no activity can be measured. The reason for the loss of activity in the experimentally prepared mutant could be that, without the hydrogen bonding to Ser132, the haloalcohol substrate does not bind, or binds improperly, to the HheC active site.

Next, the importance of the hydrogen bond that the nucleophile forms with the backbone amide of Leu178 was

tested by constructing a model in which the Leu178 amide was changed into an ester bond (the model is referred to as Leu178NH \rightarrow O; Figure 5). The optimized transition states for attack of cyanide or azide at C α and C β are shown in the Supporting Information. The calculated energies are shown in Table 2, and the critical distances are listed in Table 3.

For cyanolysis of RSO, the β -transition state exhibits optimized distances that are similar to the wild-type model. The calculated barrier is 6.5 kcal/mol, also very close to the wild-type model. Attack at C α , however, has a barrier of 9.1 kcal/mol (1.5 kcal/mol lower than that for the wild-type model), which reduces the difference between the β - and α -attacks to 2.6 kcal/mol, 1.0 kcal/mol smaller than that for the wild-type model (Table 2).

Similarly, the effect of the Leu178NH \rightarrow O mutation was examined on the azidolysis reaction. It is calculated that the barriers for attack at both C α and C β are raised compared to the wild-type model, to 10.4 and 10.5 kcal/mol, respectively (Table 2). The difference of +0.1 kcal/mol is thus 0.6 kcal/mol smaller than that for the wild-type (−0.5 kcal/mol; see Table 2). These results indicate that the backbone amide of Leu178 has quite a small effect on the regioselectivity of HheC.

The optimized transition states for the wild-type model indicate that the backbone of Pro175 interacts with a hydrogen atom on the β -carbon of RSO (Figures 2 and 3). This interaction is stronger at the β -transition state than at the α -transition state. In the azidolysis reaction, the distance from the carbonyl oxygen to the C β -hydrogen is 2.06 Å at the β -TS and 2.40 Å at the α -TS. In the cyanolysis reaction, these distances are 2.15 Å and 2.31 Å, respectively. The interaction of the Pro175 carbonyl with the C β -hydrogen seems thus to provide a stabilizing effect to the emerging positive charge on C β , thereby facilitating ring opening at this carbon.

To test this hypothesis, we replaced the CO backbone of Pro175 with a CH₂ moiety (Figure 5). With the Pro175CO \rightarrow CH₂ model, the critical distances at the optimized transition states for attack of cyanide at both C α and C β are quite similar to those in the wild-type model (Table 3; the optimized TS structures can be found in Supporting Information). The barrier for α -attack is computed to 10.8 kcal/mol, similar to the wild-type model (10.6 kcal/mol). However, for β -attack, the barrier is 8.5 kcal/mol, which is an increase of 1.5 kcal/mol compared to that in the wild-type model, indicating that the backbone carbonyl of Pro175 indeed has a role in stabilizing attack at the β -carbon.

Similar results were obtained for the azidolysis of RSO in the Pro175CO \rightarrow CH₂ model. The barriers for attack at C α and C β are computed to 11.2 and 11.5 kcal/mol, respectively (Table 2). The regioselectivity has thus changed from −0.5 kcal/mol in the wild-type model to +0.3 kcal/mol in the Pro175CO \rightarrow CH₂ model. These results thus show that the Pro175 carbonyl by its interaction with the β -proton of the substrate contributes the regioselectivity of epoxide opening in HheC.

The final modification we have done concerns the Tyr187 residue, which is a part of the halide binding site. This residue seems to provide rigidity to the halide binding site through its side chain interaction with Asn176. It has previously been suggested that this interaction stabilizes the overall confor-

mation of the HheC halide binding site (4, 26). We prepared an HheC active site model in which the Tyr187 side chain was removed from the model. (This would be analogous to a Tyr \rightarrow Gly mutation.)

In the optimized reactant of this mutant (called RmTyr187) with cyanide, the position of the nucleophile has changed somewhat compared to the wild-type model, resulting in a stronger interaction with the backbone NH of Tyr177. The distance from the cyanide nitrogen to the hydrogen of the Tyr177 amide is 2.73 Å in the wild-type (Figure 1), while in the RmTyr187 model, this distance is only 2.10 Å. This indicates that Tyr187 has an effect on the position of cyanide. The optimized transition states for cyanolysis in the RmTyr187 model have computed barriers of 7.9 and 7.8 kcal/mol for attack at C α and C β , respectively (Table 2). The regioselectivity is thus drastically reduced by the removal of the Tyr187 side chain. In terms of regioselectivity, this mutant behaves almost like that in the nonenzymatic case (see previous section).

Similar results were found for the azidolysis reaction. The computed barriers are 9.2 kcal/mol for azide attack at C α and 11.6 kcal/mol for azide attack at C β . The difference is thus 2.4 kcal/mol, which is very similar to the value obtained with the nonenzymatic phenol-catalyzed model (+2.8 kcal/mol, Table 2).

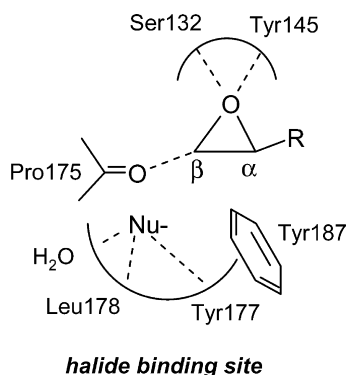
For both azidolysis and cyanolysis, Tyr187 can thus be identified as being critical for the observed change in regioselectivity in going from the phenol-catalyzed to the HheC active site model. Tyr187 seems to sterically hinder the nucleophile from approaching the α -position of RSO, thereby making attack at the β -carbon more favorable. In the absence of Tyr187, the nucleophile can reach the α -position of RSO more freely, and electronic factors will instead dominate the regioselectivity. It can be imagined that other alterations that cause large disruption of the halide binding site are also likely to induce effects similar to the removal of the Tyr187 side chain.

CONCLUSIONS

The epoxide-opening reaction of haloalcohol dehalogenase HheC from *Agrobacterium radiobacter* AD1 was investigated theoretically. The cyanolysis and azidolysis of (*R*)-styrene oxide (RSO) were studied with a large active site model based on the crystal structure of HheC (4). In the present study, we assumed that the reaction mechanism of the epoxide-opening reaction is the reverse of the proposed dehalogenation reaction (Scheme 2) (3). The barriers and reaction energies calculated for both the cyanolysis and azidolysis reactions confirm this assumption by demonstrating the energetic feasibility of the mechanism. The proposed catalytic triad indeed mediates the epoxide opening reaction of HheC. Ser132 binds the substrate and is important for reduction of the barrier by providing stabilization to the emerging oxyanion. Tyr145 acts as a general acid, donating a proton to the epoxide. In our calculations, the proton transfer was found to occur concertedly with nucleophilic attack on the epoxide. Arg149 interacts with Tyr145, thereby promoting its role as general acid.

Theoretical analysis of the regioselectivity of RSO opening with CN[−] and N₃[−] shows that the active site model used in the present study very satisfactorily reproduces the regiose-

Scheme 4: Schematic Illustration of Effects Influencing the Regioselectivity of HheC-mediated Epoxide Opening^a



^a These include positioning of the nucleophile and the substrate, steric hindrance caused by Tyr187, and electrostatic stabilization mediated by the backbone of Pro175.

lectivity of HheC. Furthermore, the active site model is of a size that permits the preparation of *in silico* mutations to gain insight into the factors governing the regioselectivity of HheC-mediated epoxide transformation. It is shown that the regioselectivity of the enzymatic epoxide opening is influenced by a combination of steric and electronic factors (Scheme 4). First, the hydrogen bonding pattern in the active site restricts the movement of the substrate and the nucleophile relative to each other. For example, the removal of the hydrogen bond from the Leu178 backbone to cyanide reduces the regioselectivity of RSO cyanolysis by 1.0 kcal/mol. Second, the backbone carbonyl of Pro175 provides electrostatic stabilization to C β , facilitating opening at this carbon. In our model, mutation of the Pro175 carbonyl reduces the regioselectivity of RSO cyanolysis by 1.3 kcal/mol. Finally, the most significant effect identified in this study is exerted by Tyr187. The Tyr187 side chain imposes steric hindrance on the nucleophile, making attack at C α less favorable. The removal of Tyr187 results in a regioselectivity that is very similar to the nonenzymatic case.

SUPPORTING INFORMATION AVAILABLE

Product geometries for the attack at C α of RSO in the HheC wild type model, geometries of the optimized transition states for all mutant models, a table with barriers and regioselectivities of RSO cyanolysis in the wild type HheC model as a function of the dielectric constant, and a table containing a comparison of the barriers using the small and the large basis sets. This material is available free of charge via the Internet at <http://pubs.acs.org>.

REFERENCES

- Nakamura, T., Nagasawa, T., Yu, F., Watanabe, I., and Yamada, H. (1994) Characterization of a novel enantioselective halohydrin hydrogen-halide-lyase. *Appl. Environ. Microbiol.* 60, 1297–1301.
- Van den Wijngaard, A. J., Reuvekamp, P. T. W., and Janssen, D. B. (1991) Purification and characterization of haloalcohol dehalogenase from *Arthrobacter* sp. strain AD2. *J. Bacteriol.* 173, 124–129.
- van Hylckama Vlieg, J. E. T., Tang, L., Lutje Spelberg, J. H., Smilda, T., Poelarends, G. J., Bosma, T., van Merode, A. E., Fraaije, M. W., and Janssen, D. B. (2001) Halohydrin dehalogenases are structurally and mechanistically related to short-chain dehydrogenases/reductases. *J. Bacteriol.* 183, 5058–5066.
- de Jong, R. M., Tiesinga, J. J., Rozeboom, H. J., Kalk, K. H., Tang, L., Janssen, D. B., and Dijkstra, B. W. (2003) Structure and mechanism of a bacterial haloalcohol dehalogenase: a new variation of the short-chain dehydrogenase/reductase fold without an NAD-(P)H binding site. *EMBO J.* 22, 4933–4944.
- Tang, L., Lutje Spelberg, J. H., Fraaije, M. W., and Janssen, D. B. (2003) Kinetic mechanism and enantioselectivity of halohydrin dehalogenase from *Agrobacterium radiobacter*. *Biochemistry* 42, 5378–5386.
- Janssen, D. B., Majerić-Elenkov, M., Hasnaoui, G., Hauer, B., and Lutje Spelberg, J. H. (2006) Enantioselective formation and ring-opening of epoxides catalysed by halohydrin dehalogenases. *Biochem. Soc. Trans.* 34, 291–295.
- Lutje Spelberg, J. H., Tang, L., van Gelder, M., Kellogg, R. M., and Janssen, D. B. (2002) Exploration of the biocatalytic potential of a halohydrin dehalogenase using chromogenic substrates. *Tetrahedron Asymmetry* 13, 1083–1089.
- Majerić-Elenkov, M., Tang, L., Hauer, B., and Janssen, D. B. (2006) Sequential kinetic resolution catalyzed by halohydrin dehalogenase. *Org. Lett.* 8, 4227–4229.
- Hasnaoui, G., Lutje Spelberg, J. H., de Vries, E., Tang, L., Hauer, B., and Janssen, D. B. (2005) Nitrite-mediated hydrolysis of epoxides catalyzed by halohydrin dehalogenase from *Agrobacterium radiobacter* AD1: a new tool for the kinetic resolution of epoxides. *Tetrahedron Asymmetry* 16, 1685–1692.
- Lutje Spelberg, J. H., van Hylckama Vlieg, J. E. T., Tang, L., Janssen, D. B., and Kellogg, R. M. (2001) Highly enantioselective and regioselective biocatalytic azidolysis of aromatic epoxides. *Org. Lett.* 3, 41–43.
- Majerić-Elenkov, M., Hauer, B., and Janssen, D. B. (2006) Enantioselective ring opening of epoxides with cyanide catalysed by halohydrin dehalogenases: a new approach to non-racemic β -hydroxy nitriles. *Adv. Synth. Catal.* 348, 579–585.
- Lutje Spelberg, J. H., van Hylckama Vlieg, J. E. T., Bosma, T., Kellogg, R. M., and Janssen, D. B. (1999) A tandem enzyme reaction to produce optically active halohydrins, epoxides and diols. *Tetrahedron Asymmetry* 10, 2863–2870.
- Haak, R. M., Tarabiono, C., Janssen, D. B., Minnaard, A. J., de Vries, J. G., and Feringa, B. L. (2007) Synthesis of enantiopure chloroalcohols by enzymatic kinetic resolution. *Org. Biomol. Chem.* 5, 318–323.
- (a) Velichkova, P., and Himo, F. (2005) Methyl transfer in glycine N-methyltransferase: A theoretical study. *J. Phys. Chem. B* 109, 8216–8219. (b) Himo, F., Guo, J.-D., Rinaldo-Matthis, A., and Nordlund, P. (2005) Reaction mechanism of deoxyribonucleotidase: a theoretical study. *J. Phys. Chem. B* 109, 20004–20008. (c) Velichkova, P., and Himo, F. (2006) Theoretical study of the methyl transfer in guanidinoacetate methyltransferase. *J. Phys. Chem. B* 110, 16–19. (d) Chen, S.-L., Fang, W.-H., and Himo, F. (2007) Theoretical study of the phosphotriesterase reaction mechanism. *J. Phys. Chem. B* 111, 1253–1255. (e) Sevastik, R., and Himo, F. (2007) Quantum chemical modeling of enzymatic reactions: the case of 4-oxalocrotonate tautomerase. *Bioorg. Chem.* 35, 444–457. (f) Hopmann, K. H., Guo, J.-D., and Himo, F. (2007) Theoretical investigation of the first-shell mechanism of nitrile hydratase. *Inorg. Chem.* 46, 4850–4856. (g) Hopmann, K. H., Hallberg, B. M., and Himo, F. (2005) Catalytic mechanism of limonene epoxide hydrolase, a theoretical study. *J. Am. Chem. Soc.* 127, 14339–14347. (h) Hopmann, K. H., and Himo, F. (2006) Theoretical study of the full reaction mechanism of human soluble epoxide hydrolase. *Chem. Eur. J.* 12, 6898–6909. (i) Hopmann, K. H., and Himo, F. (2006) Insights into the reaction mechanism of soluble epoxide hydrolase from theoretical active site mutants. *J. Phys. Chem. B* 110, 21299–21310.
- (a) Lee, C., Yang, W., and Parr, R. G. (1988) Development of the Colle-Salvetti correlation-energy formula into a functional of the electron density. *Phys. Rev. B* 37, 785–89. (b) Becke, A. D. (1988) Density-functional exchange-energy approximation with correct asymptotic behavior. *Phys. Rev. A* 38, 3098–3100. (c) Becke, A. D. (1992) Density-functional thermochemistry. I. The effect of the exchange-only gradient correction. *J. Chem. Phys.* 96, 2155–2160. (d) Becke, A. D. (1992) Density-functional thermochemistry. II. The effect of the Perdew–Wang generalized-gradient correlation correction. *J. Chem. Phys.* 97, 9173–77. (e) Becke, A. D. (1993) Density-functional thermochemistry. III. The role of exact exchange. *J. Chem. Phys.* 98, 5648–5652.
- Frish, M. J., Trucks, G. W., Schlegel, H. B., Scuseria, G. E., Robb, M. A., Cheeseman, J. R., Montgomery, J. A., Jr., Vreven, T., Kudin, K. N., Burant, J. C., Millam, J. M., Iyengar, S. S., Tomasi, J., Barone,

- V. Mennucci, B. Cossi, M. Scalmani, G. Rega, N. Petersson, G. A. Nakatsuji, H. Hada, M. Ehara, M. Toyota, K. Fukuda, R. Hasegawa, J. Ishida, M. Nakajima, T. Honda, Y. Kitao, O. Nakai, H. Klene, M. Li, X. Knox, J. E. Hratchian, H. P. Cross, J. B. Adamo, C. Jaramillo, J. Gomperts, R. Stratmann, R. E. Yazyev, O. Austin, A. J. Cammi, R. Pomelli, C. Ochterski, J. W. Ayala, P. Y. Morokuma, K. Voth, G. A. Salvador, P. Dannenberg, J. J. Zakrzewski, V. G. Dapprich, S. Daniels, A. D. Strain, M. C. Farkas, O. Malick, D. K. Rabuck, A. D. Raghavachari, K. Foresman, J. B. Ortiz, J. V. Cui, Q. Baboul, A. G. Clifford, S. Cioslowski, J. Stefanov, B. B. Liu, G. Liashenko, A. Piskorz, P. Komaromi, I. Martin, R. L. Fox, D. J. Keith, T. Al-Laham, M. A. Peng, C. Y. Nanayakkara, A. Challacombe, M. Gill, P. M. W. Johnson, B. Chen, W. Wong, M. W. Gonzalez, C., and Pople, J. A. (2003) Gaussian 03, revision B.03, Gaussian, Inc., Pittsburgh, PA.
17. (a) Klamt, A., and Schüürmann, G. (1993) COSMO: a new approach to dielectric screening in solvents with explicit expressions for the screening energy and its gradient. *J. Chem. Soc., Perkin. Trans. 2*, 799–805. (b) Andzelm, J., Kölmel, C., and Klamt, A. (1995) Incorporation of solvent effects into density functional calculations of molecular energies and geometries. *J. Chem. Phys.* 103, 9312–9320. (c) Barone, V., and Cossi, M. (1995) (1998) Quantum Calculation of Molecular Energies and Energy Gradients in Solution by a Conductor Solvent Model. *J. Phys. Chem. A* 102, 2001. (d) Cossi, M., Rega, N., Scalmani, G., and Barone, V. (2003) Energies, structures, and electronic properties of molecules in solution with the C-PCM solvation model. *J. Comput. Chem.* 24, 669–681.
18. March, J. (1992) *Advanced Organic Chemistry: Reactions, Mechanism and Structure*, 4th ed., John Wiley & Sons, New York.
19. Iranpoor, N., Firouzabadi, H., and Shekarize, M. (2003) Micellar media for the efficient ring opening of epoxides with CN^- , N_3^- , NO_3^- , NO_2^- , SCN^- , Cl^- and Br^- catalyzed with $\text{Ce}(\text{OTf})_4$. *Org. Biomol. Chem.* 1, 724–727.
20. Chini, M., Crotti, P., Favero, L., and Macchia, F. (1991) Easy direct stereo- and regioselective formation of β -hydroxy nitriles by reaction of 1,2-epoxides with potassium cyanide in the presence of metal salts. *Tetrahedron Lett.* 32, 4775–4778.
21. Srinivas, B., Kumar, V. P., Sridhar, R., Surendra, K., Nageswar, Y. V. D., and Rama Rao, K. (2007) Regioselective nucleophilic opening of epoxides and aziridines under neutral conditions in the presence of β -cyclodextrin in water. *J. Mol. Catal. A: Chemical* 261, 1–5.
22. Onaka, M., Ohta, A., Sugita, K., and Izumi, Z. (1995) New application of solid base to regioselective ring openings of functionalized epoxides and oxetanes with cyanotrimethylsilane. *Appl. Catal., A* 125, 203–216.
23. Mirmashhori, B., Azizi, N., and Saidi, M. R. (2006) A simple, economical, and highly efficient synthesis of β -hydroxynitriles from epoxide under solvent free conditions. *J. Mol. Catal. A: Chem.* 247, 159–161.
24. Van de Weghe, P., and Collin, J. (1995) Ring opening reactions of epoxides catalyzed by samarium iodides. *Tetrahedron Lett.* 36, 1649–1652.
25. Fringuelli, F., Piermatti, O., Pizzo, F., and Vaccaro, L. (1999) Ring opening of epoxides with sodium azide in water. A regioselective pH-controlled reaction. *J. Org. Chem.* 64, 6094–6096.
26. Tang, L., Pazmiño, D. E. T., Marco W. Fraaije, M. W., de Jong, R. M., Dijkstra, B. W., and Janssen, D. B. (2005) Improved catalytic properties of halohydrin dehalogenase by modification of the halide-binding site. *Biochemistry* 44, 6609–6618.

BI800001R